



**Citation:** Author (2024). IoT technology as a support tool for the calculation of Crop Water Stress Index in a *Vitis vinifera* L. cv. Chardonnay vineyard in Northern Italy. *Italian Journal of Agrometeorology* (2): 65-80. doi: 10.36253/ijam-2747

**Received:** May 2, 2024

**Accepted:** October 22, 2024

**Published:** December 30, 2024

© 2024 Author(s). This is an open access, peer-reviewed article published by Firenze University Press (<https://www.fupress.com>) and distributed, except where otherwise noted, under the terms of the CC BY 4.0 License for content and CC0 1.0 Universal for metadata.

**Data Availability Statement:** All relevant data are within the paper and its Supporting Information files.

**Competing Interests:** The Author(s) declare(s) no conflict of interest.

**ORCID:**

CM: 0009-0004-6271-1200

MR: 0000-0003-3228-4557

RZ: 0000-0003-3832-6033

## IoT technology as a support tool for the calculation of Crop Water Stress Index in a *Vitis vinifera* L. cv. Chardonnay vineyard in Northern Italy

CECILIA MATTEDI<sup>1</sup>, MIRCO RODEGHIERO<sup>2</sup>, ROBERTO ZORER<sup>3</sup>

<sup>1</sup> Agrometeorology and Irrigation Unit, Technology Transfer Center, Fondazione Edmund Mach, Via E. Mach 1, 38098 San Michele all'Adige (TN), Italy

<sup>2</sup> C3A - Center Agriculture Food Environment, University of Trento, 38098 San Michele all'Adige (TN), Italy

<sup>3</sup> Digital Agriculture Unit, Research and Innovation Centre, Fondazione Edmund Mach, Via E. Mach 1, 38098 San Michele all'Adige (TN), Italy

\*Corresponding author. E-mail: [cecilia.mattedi@fmach.it](mailto:cecilia.mattedi@fmach.it)

**Abstract.** Nowadays agriculture is one of the main sectors affected by climate change. The continuous increase of temperature and drought periods are posing serious problems in terms of shift of plants' phenological phases and a reduction of crop yield quantity and quality. Among the indexes used to assess plant water status, the Crop Water Stress Index (CWSI) is one of the most studied due to its ease of calculation. We performed a study in a vineyard in Trentino (San Michele all'Adige, Northern Italy) where we took advantage of IoT Technology to build a device to measure leaf temperature and automatically calculate the CWSI. Parameters necessary to determine the CWSI were the temperature of a non-transpiring leaf, (artificial 3D printed black leaf), and the temperature of a fully-transpiring leaf (wet bulb temperature of the air). We compared various types of thermometers to measure temperatures of the real leaves, and with repeated measuring campaigns performed during the summer of 2022 we could obtain spatial maps of CWSI that could highlight the stress levels of the vineyard and therefore address the irrigation management in a context of precision agriculture.

**Keywords:** drought stress, precision agriculture, leaf temperature, irrigation management, CWSI.

---

### HIGHLIGHTS

- An IoT based approach was tested to assess leaf temperature in order to calculate the real time Crop Water Stress Index.
- A prototype was tested during summer 2022 in a vineyard in San Michele all'Adige (TN) during a period of strong drought.
- Different thermometers were compared to measure leaf temperature.

- The derived data allowed the creation of maps of CWSI which can be used in precision agriculture to save water and increase WUE.
- Some weak points of the system are discussed in order to improve the accuracy in the estimation of CWSI.

## 1. INTRODUCTION

Year 2022 has been one of the warmest years on record in Europe since 1950 (Global Climate Highlights 2023, 2024), with a temperature anomaly of  $+0.85\text{ }^{\circ}\text{C}$  with respect to the 1991-2020 reference period average. The consequences of the ongoing Climate Change are heavily affecting human systems and ecosystems, and one of the hardest hit sectors is agriculture. The increase in air temperature has proven to be responsible for a shift in the phenological phases of the crops: for grapevine cultivation, the anticipation of the onset of the growing season and bud break has been observed in different areas of Italy and has been highlighted by several studies (Caffarra and Eccel, 2011; Venios et al., 2020). On one hand, the anticipation of the onset of the growing season can bring farmers to cultivate longer-maturing crops or more crop cycles altogether. On the other hand, temperature increases are more likely responsible for a reduction in yield and crop quality (Adams et al., 1998). Another consequence of a rapidly changing climate is the imbalance of the water regime, that is showing a decrease in annual rainfall and a higher frequency of extreme events like floods and droughts. According to the 6<sup>th</sup> Assessment Report of the IPCC (Intergovernmental Panel On Climate Change - IPCC, 2023), in the dry summer climates characterizing the Mediterranean area drought phenomena will be enhanced. Thus, responsible management of the water resource is one of the main challenges for the next few years, in order to provide crops with the right amount of irrigation without compromising crop yield and quality.

Plants are organisms directly affected by changes in atmospheric variables such as temperature and precipitation. Droughts are often linked to periods with particularly high temperatures (Mathur et al., 2014), and the effects of these phenomena are mainly appreciable in leaves and roots, which are the most sensible plant organs (Wu et al., 2022). The first-line plant defense against periods of water scarcity or high temperatures is stomatal closure (Venios et al., 2020), that prevents an excessive loss of water vapor through the leaf stomata. This is followed by a decrease in stomatal conductance (Buckley, 2019) and gas exchange (both water vapor and

$\text{CO}_2$ ), that leads to a reduction of photosynthetic activity, plant growth and lower crop production and yield quality (Zhao et al., 2020).

Another consequence of stomatal closure is the increase of leaf temperature. Most of the solar radiation absorbed by the leaf is usually dissipated through sensible (responsible for temperature rise) and latent (transpiration) heat fluxes, but with limited stomatal conductance the latter is drastically reduced and the leaf overheats due to insufficient heat loss (Chaves et al., 2016). The overheating then compromises the photosynthetic processes, and the quality of the crops (Venios et al., 2020) is negatively affected. Plants can activate tolerance mechanisms to overcome short periods of stress, without reporting serious damages (Chaves et al., 2016), but repeated overheating can lead to leaf damage, visible as bleaching, up to desiccation and phylloptosis. As heatwaves accompanied by dry periods will become more frequent, Precision Agriculture practices can be implemented to improve the water use efficiency through irrigation time scheduling and modifying the irrigation rate depending on soil and plant characteristics (Nair et al., 2013; Bwambale et al., 2022). The Internet of Things (IoT) is one of the emerging technologies that complement Precision Agriculture practices, consisting in a network of physical objects interconnected via the Internet, that collects and stores the data recorded by the sensors (Esposito et al., 2022). It allows real-time collection and analysis of useful environmental information, which can be transmitted back to farmers

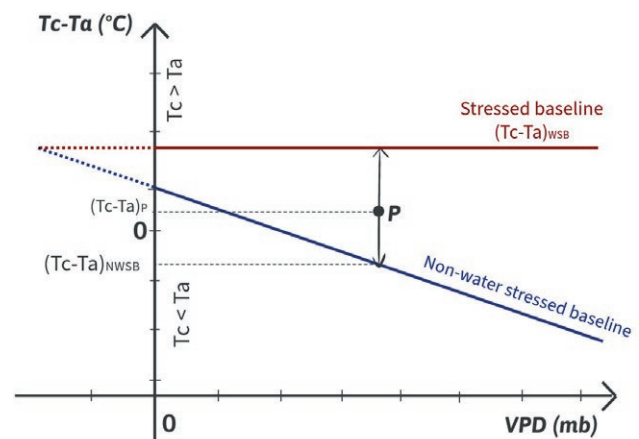


**Figure 1.** Schematic representation of CWSI (Crop Water Stress Index). Point *P* represents the current crop status, the “Non-Water Stressed Baseline” (NWSB) denotes the crop at potential evapotranspiration and the “Stressed Baseline” (WSB) denotes the crop in a fully stressed condition.  $T_c$  and  $T_a$  are canopy and air temperature respectively. VPD is the Vapor Pressure Deficit between the canopy and the air (plot adapted from Nanda et al., 2018).

via the Internet, acting as a support for the control of growing conditions of the crops and managing irrigation practices.

Many indexes have been developed to assess plant water status. The CWSI (Crop Water Stress Index) was first introduced in 1981 (Idso et al., 1981; Jackson et al., 1981) as an extension of the stress-degree-day concept, in order to have an index that could be independent of environmental factors other than soil moisture (like air vapor pressure, net radiation and wind speed). The expression was developed based on leaf temperature values taken in three different crop states: potential evapotranspiration, stress conditions and current conditions (Idso et al., 1981). These temperatures were plotted in a graph with the difference between canopy temperature ( $T_c$ ) and air temperature ( $T_a$ ) ( $T_c - T_a = CATD$ ) on the y-axis and vapor pressure deficit (VPD) on the x-axis (Fig. 1). The measurements taken in the optimal state of potential evaporation followed a linear pattern (non-water stress baseline, NWSB), whereas the measurements taken in stress conditions were aligned along a horizontal line (stressed baseline, WSB). At a specific VPD and CATD value (point P in Fig. 1), the CWSI was defined as the ratio of 2 vertical segments: the distance between point P and the NWSB (blue line) and the total path between NWSB and WSB (red line):

$$CWSI = \frac{(T_c - T_a)_P - (T_c - T_a)_{NWSB}}{(T_c - T_a)_{WSB} - (T_c - T_a)_{NWSB}} \quad (1)$$

The CWSI value ranges from 0 to 1, representing respectively the state of no water stress (potential evapotranspiration) and the state of severe stress (suppressed transpiration).

The determination of the baselines is not straightforward, as they vary with respect to plant species and the crop growth stages (Idso, 1982). A theoretical formulation was developed from the energy balance of a crop canopy (Jackson et al., 1981):

$$CWSI_t = \frac{\gamma \left(1 + \frac{r_c}{r_a}\right) - \gamma \left(1 + \frac{r_{cp}}{r_a}\right)}{\Delta + \gamma \left(1 + \frac{r_c}{r_a}\right)} \quad (2)$$

$$(T_c - T_a)_{NWSB} = \frac{r_a R_n \gamma VPD}{\rho C_p (\Delta + \gamma)^2} \quad (3)$$

$$(T_c - T_a)_{WSB} = \frac{r_a R_n}{\rho C_p} \quad (4)$$

being  $\gamma$  the psychrometric constant,  $r_c$  and  $r_a$  the canopy resistance and the aerodynamic resistance to vapor transport respectively,  $r_{cp}$  the canopy resistance evaluated at full canopy transpiration,  $\Delta$  the slope of the saturation vapor pressure-temperature relation,  $R_n$  the net radiation,  $\rho$  the air density, and VPD the Vapor Pressure Deficit.

In an easier calculation approach CWSI was formulated based only on infrared temperature measurements of individual leaves and of reference surfaces, specifically of wet and dry reference surfaces ( $T_{wet}$  and  $T_{dry}$ ; Jones, 1999; Katimbo et al., 2022).

$$(T_c - T_a)_{NWSB} = T_{wet} - T_a \quad (5)$$

$$(T_c - T_a)_{WSB} = T_{dry} - T_a \quad (6)$$

$$CWSI = \frac{(T_c - T_a)_P - (T_c - T_a)_{NWSB}}{(T_c - T_a)_{WSB} - (T_c - T_a)_{NWSB}} = \frac{T_c - T_{wet}}{T_{dry} - T_{wet}} \quad (7)$$

With this formulation the CWSI could be calculated in an easier way and with a restricted amount of variables, by measuring at the same time the canopy temperature  $T_c$ , the temperature of a reference wet surface  $T_{wet}$  and the temperature of a dry reference surface  $T_{dry}$  (Eq. 7).

A consistent number of studies investigated possible methods to determine these reference values. They have been determined by covering real leaves with a layer of coating like petroleum jelly or Vapor Gard to block evapotranspiration for the measurement of  $T_{dry}$ , and with a thin layer of water to measure  $T_{wet}$  (Leinonen and Jones, 2004; Ouerghi et al., 2014; Poblete-Echeverría et al., 2017). Artificial reference surfaces mimicking real leaves have also been realized using water absorbing cloths (Maes et al., 2016), or soaked fabric and dry fabric made of Styrofoam to determine respectively  $T_{wet}$  and  $T_{dry}$  (Katimbo et al., 2022). Other tests mimicking artificial leaves used cellulose paper-based surfaces (Apolo-Apolo et al., 2020), green plastic-made hemispherical surfaces (Jones et al., 2018) and wet viscose-polyester fabric covering a polystyrene float (Meron et al., 2010).

More recent experimentation tested also neural network models to determine the lower baseline and develop a CWSI based IoT irrigation DSS (Decision Supporting System), obtaining a very reliable DSS but way too much expensive for the practical commercial application (King and Shellie, 2023). This is a common problem for this kind of experiments, as they bring valuable results but are not affordable for a systematic use in the field. On the other hand, sensors are usually expensive and do not allow a continuous, low cost and wide monitoring of the CWSI equation parameters (Fuentes-Peñailillo et al., 2024).

This study was aimed to 1) compare different instruments to measure leaf temperature ( $T_{leaf}$ ) and 2) figure out the best method to assess the dry and wet reference temperatures ( $T_{wet}$  and  $T_{dry}$ ) for the computation of the Crop Water Stress Index (CWSI). Subsequently, the relation between CWSI and stomatal conductance  $g_{sw}$  was investigated. Finally, a spatial interpolation of CWSI measured during the mapping experiments was performed in Geographic Information System (GIS) software to analyze the spatial variability of the plant water stress degree in the different parts of the vineyard. The final goal of this study was to develop an IoT station for an implementation of the Crop Water Stress Index that could be affordable for the continuous monitoring of the crop water status, by means of low cost sensors and the connection to a LoRaWan network.

## 2. MATERIALS AND METHODS

### 2.1. Study site

The present research work was conducted at the Molini Bassi vineyard (Fig. 2a) of the Fondazione Edmund Mach (FEM), former Istituto Agrario di San Michele all'Adige (Trento, Italy). It is located on the eastern side of the Adige Valley, at an altitude varying between 220 and 230 m a.s.l. It is oriented in the South-West direction (about  $241^\circ$  North) and, due to the hilly landscape and the North-South extension of the Adige Valley, the vines can benefit from the sunlight for about 10.4 hours on average over the growing season. The vineyard has an extension of

8400 m<sup>2</sup> with 77 rows oriented  $15^\circ$  to the North-East/South-West direction. *Vitis vinifera* L. cv. Chardonnay, grafted onto SO4 rootstock, was planted during 2020. Vines are spaced to a fixed distance of  $0.8 \times 2$  m VSP trained with guyot-type pruning system. In particular, this research work was performed in rows going from number 8 to 13 with Chardonnay (clone 809) and from 14 to 17 with clone 78 (Fig. 2a). During 2021, the vineyard was provided with a series of facilities aimed at the installation of prototype instruments developed by FEM or in collaboration with national and international companies and research institutes. At the moment, the vineyard is equipped with 220 V AC mains power and low-voltage (12V DC) power supply lines, WiFi and LoRaWAN coverage for receiving data via long-distance radio signals from Internet of Things-IoT sensors, dataloggers, and microcontrollers.

### 2.2. Leaf temperature measurements

The assessment of leaf temperature was a crucial aspect of this work and therefore several independent sensors were used to measure leaf temperature:

- **CWSI slave station (IRMLX, Fig. 3):** it is a prototype of Crop Water Stress Index device, designed and assembled by FEM researchers, consisting in a portable box (WP11-15-4 G Takachi Electric Industrials enclosure of dimensions 110×150×40 mm) equipped with a MLX90614 infrared sensor (MELEXIS, Ypres, Belgium) for non-contact temperature measurements connected to an Arduino MKR WAN 1310 microcontroller. It is also supplied with an Arduino MKR GPS shield that provides the coor-

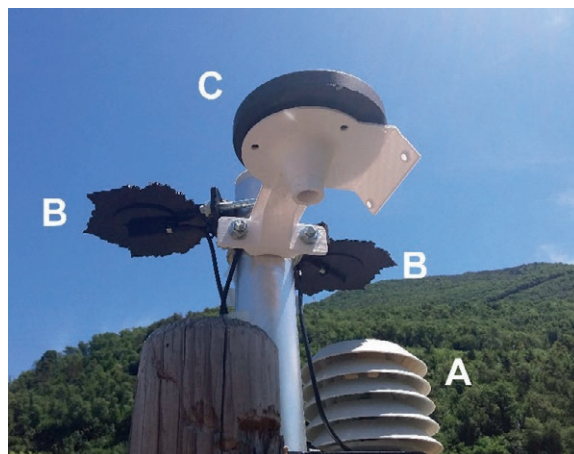
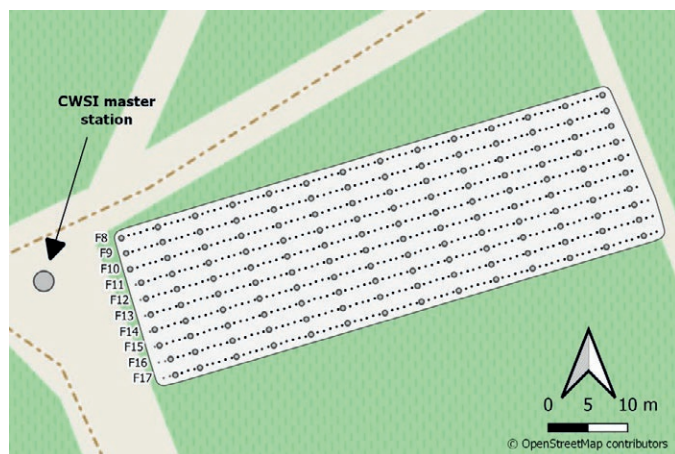


**Figure 2.** (a) Map of the study site (white area). The grey dots correspond to the poles and the black dots indicate the position of each vine plant. Numbers of the plant rows are shown on the left side. (b) CWSI master station equipped with: A) a thermo-hygrometer; B) two black artificial leaves; C) an aluminum oxide disk.



Figure 3. (a) Setup of CWSI slave station. (b) CWSI slave station measurements.

dinates of the sampling position. In addition the leaf temperature is sent back in the data array (payload) to the LoRaWAN Gateway by means of radio transmission (868 MHz). A GT-P3100 Samsung Galaxy Tab 2 7.0 tablet is mounted on top of the box, allowing the instrument to be powered and displaying via a serial monitor app the measured variables: temperature of the target (the leaf), the temperature of the sensor itself and its GPS coordinates. The infrared sensor has an accuracy of 0.5 °C and a resolution of 0.02 °C. The sensor is activated by pressing a red button located on the right side of the box, holding the position of the sensor for a couple of seconds to properly register the temperature value.

- **Licor LI-600 (Li600) Porometer/Fluorometer (LI-COR Inc., Lincoln, NE, USA):** Leaf temperature was measured at the same time as stomatal conductance ( $g_{sw}$ ) by means of an infrared thermal sensor integrated in the instrument itself; the data were recorded in a file together with the time of acquisition, therefore allowing the synchronization with the measurements made with the other instruments.
- **A spare Type E thermocouple (TCext) (Li6400-04; LI-COR Inc., Lincoln, NE, USA):** part of the Li6400-40 leaf chamber fluorometer, with a 10 cm cable length and connected to a CR10X Datalogger

(Campbell Scientific, Logan, UK) acquiring leaf temperature values every minute and averaging them every 15 minutes.

- **Type T thermocouple (TCint) (1m length cable, 1/0.2 mm Diameter, RS Pro Components, Belgium):** was connected to the CR10X Datalogger as well; values were recorded every 60 seconds and averaged every 15 minutes.
- a portable **62 MAX Mini Infrared Thermometer (IR62)** (Fluke Corporation, Everett, WA, USA) was used to get leaf temperature values in the same leaf previously measured by the Licor LI-600.

### 2.3. CWSI master station

An essential part of the setup was represented by the CWSI Master station, consisting of an Arduino MKR WAN 1310 microcontroller and several sensors mounted on a 2.3 m high pole located at a distance of about 7 meters from the north-western corner of the vineyard (Fig. 2a). The sensors included a digital thermo-hygrometer (AM2315 - Encased I2C Temperature/Humidity Sensor; Adafruit Industries, NY, USA) recording temperature and relative humidity of the surrounding air, hosted in a 3D printed (white Co-PolyEster CPE) radiation shield (Fig. 2b, A); 3 encapsulated DS18B20 digital

temperature sensors (DFR0198, DFRobot, Shanghai) installed into 3 different artificial media, which should best mimic the state of a non transpiring leaf: the first in a black painted 3D printed leaf made of PolyAmide 12 (PA12; Fig. 2b, B), the second into a black 3D printed leaf made of black CPE (Fig. 2b, B), and, finally, the third (DS18B20 temperature probe) was placed in a black painted aluminum oxide disk, part of an Everest Inter-science Model 1000 Calibration Source (Fig. 2b, C).

Other meteorological variables were derived through some simple calculations starting from the measured air temperature ( $T_{air}$ ) and relative humidity ( $RH$ ):

- Dew point temperature: following the derivation of Lawrence (2005):

$$T_{dew} = \frac{B \alpha(T_{air}, RH)}{A - \alpha(T_{air}, RH)} \quad (8)$$

where  $A = 17625$  and  $B = 243.04^\circ\text{C}$  are constants and  $\alpha$  is defined as a function of  $T_{air}$  and  $RH$  (Lawrence, 2005):

$$\alpha(T_{air}, RH) = \ln\left(\frac{RH}{100}\right) + \frac{A T_{air}}{B + T_{air}} \quad (9)$$

- Wet bulb temperature: computed with the Stull formula (Stull, 2011):

$$T_{wb} = T_{air} \arctan(0.151977(RH + 8.313659)^{0.5}) + \arctan(T_{air} + RH) - \arctan(RH - 1.6763311) + 0.00391838 RH^{1.5} + \arctan(0.23101 RH) - 4.686035 \quad (10)$$

#### 2.4. Data transmission

The CWSI master station was equipped with an Arduino MKR WAN 1310 microcontroller, adding a LoRa/LoRaWAN connectivity to the station (license-free radio frequency bands of 868 MHz) and allowing a LoRa communication with the CWSI Slave station, together with the use of a LoRaWAN protocol to send back the data to both the gateway and the online IoT-service. In fact, the Crop Water Stress Index station was registered into a cloud service provided by The Things Stack (The Things Industries), an open source LoRaWAN Network Server which offers a set of open tools and a global, open network to build IoT applications at low cost, featuring maximum security and ready to scale. The presence of a nearby registered gateway (The Things Indoor Gateway - TTIG, The Things Industries) connected to the internet

through a 4G LTE WiFi router (RUT240, Teltonika Networks, Vilnius, Lithuania) was required for the transmission of the data. Whenever the red button of the CWSI Slave station was pressed, a LoRa digital radio signal containing the data (leaf and sensor temperature, time and device position) was sent to the CWSI master station, activating all the sensors of the CWSI master station. The registered data were then sent as an encoded array of bytes (payload) through LoRaWAN protocols to the TTIG gateway and back to The Things Stack-TTS IoT-cloud service. The Things Stack offers a cloud storage service with a data retention period of 24 hours, an Hypertext Transfer Protocol (HTTP) integration and Message Queuing Telemetry Transport (MQTT) service to grant access and download of the data.

#### 2.5. Field monitoring activities

Two types of field activities were performed during the summer of year 2022, between July and August: mapping sessions and calibration sessions. The mapping campaigns were executed on July 19<sup>th</sup>, July 25<sup>th</sup>, August 9<sup>th</sup> and consisted in monitoring the state of a vineyard subplot, with the aim to create spatial maps of CWSI. For every session a total of 130 leaf temperatures were recorded, choosing 13 representative leaves of the south-facing side of each row (i.e. one located in the middle between two poles). The sampling sequence started on the western side of row number 8 of the vineyard, going to the east direction; the following row was sampled going backward in the opposite direction, continuing in this way for all the 10 vineyards rows.

The target leaf was chosen according to the following criteria: mature stage, well-developed, healthy and lit by the sun. The leaf temperature was measured in the same way on the superior lamina, between the mid-vein and the superior lateral vein. For every leaf, three temperature values were collected, using three different instruments: LI-600 Porometer/Fluorometer (acronym: Li600), CWSI Slave station (acronym: IRMLX), IR thermometer (acronym: IR62). In order to have the most reliable values of temperature, they were measured in the same spot of the leaf area, the sequence of the instruments was kept constant and the time of measurement was kept as short as possible, to avoid sensible changes in leaf temperature.

The measurements were performed in days with clear sky conditions (Poirier-Pocovi and Bailey, 2020) and in the warmest hours of the day (Idso et al., 1981), i.e. an hour and a half after solar noon. At this time of the day plants usually reach their maximum stress condition and the lowest stomatal conductance, therefore being a good time

for quantifying the crop water stress (Jackson et al., 1981).

An additional mapping session was executed on August 23<sup>rd</sup>, to assess the spatial variability of air temperature and relative humidity within the vineyard as compared to the master station, positioned just outside the rows in an open position. MP100A thermo-hygrometer (Rotronic Italia S. R. L., Rho, Milano) was brought to the field, installed on a 1.5 m portable rod and connected to a Datalogger (CR10x, Campbell Scientific, Logan, UK) programmed to record temperature and relative humidity values every minute. During the measurement of the leaf temperature, the rod was leaned against the canopy in the proximity of the measured leaf with the aim of characterizing the micro-climate of the canopy. After the end of the mapping session the collected data were synchronized (based on time) with those of the CWSI master station in order to compare the climate inside and outside the vineyard. The second type of field activity consisted in calibration campaigns to compare the accuracy in leaf temperature measurement of the instruments used during the mapping session. The calibration campaigns were conducted on August 25<sup>th</sup> and August 29<sup>th</sup> following the same procedure: one representative leaf (healthy, mature and sun-lit) was selected and monitored during both days. It was located in row number 10 of the vineyard, between the third and the fourth pole. Leaf temperatures were measured with two thermocouples: one of them (RS PRO type T thermocouple, referred as internal thermocouple, TCint) was inserted in the mid-vein of the inferior lamina of the leaf, and the other one (LI-6400/XT type E thermocouple, referred as external thermocouple, TCext) was positioned in contact with the inferior lamina. The thermocouples were both connected to a CR10X Datalogger that was set to log data with an interval of 1 minute. Leaf temperatures were collected also with the instruments used in the mapping sessions with a time interval of 15 minutes as well. The two sessions started around 9:30 (CEST) in the morning and ended in the afternoon, when the leaf got shaded by the canopy and a stormy

cloud was approaching.

Further details about the start and end time of the mapping sessions are given in Table 1.

### 2.6. Leaf temperature correction

According to the literature, the instrument which best approximates the real leaf temperature is the internal thermocouple (Halbritter et al., 2020): being inserted in the inferior lamina of the leaf, it does not affect other parameters influencing leaf temperature such as solar radiation, leaf angle or the boundary layer. Every instrument was compared to TCint with a scatter plot and a linear regression fit (Martínez et al., 2017; Kim et al., 2018), calculating also the coefficient of determination ( $R^2$ ) and the statistical significance ( $p < 0.05$ ). New temperature values for each instrument were calculated ( $y_{new}$ ) based on the coefficients of the regression line:

$$y_{new} = x_{old} = (y_{old} - b)/a \tag{11}$$

where  $a$  is the slope and  $b$  the intercept of the linear regression line. This process was repeated for both the mapping and the calibration sessions.

### 2.7. Crop Water Stress Index calculation

The Crop Water Stress Index was calculated using Eq. 7 replacing the canopy temperature  $T_c$  with a single leaf temperature  $T_{leaf}$

$$CWSI = \frac{T_{leaf} - T_{wet}}{T_{dry} - T_{wet}} \tag{12}$$

being  $T_{wet}$  the wet reference temperature, expressed by the wet bulb temperature of the air (Eq. 10) and  $T_{dry}$  the dry reference temperature measured by the black reference devices on the CWSI master station. Every  $T_{leaf}$  calculated with the instruments listed previously, was

**Table 1.** Field activities calendar, with start and end time of each measuring session and type of instruments used. Li600 (LI-600 Porometer/Fluorometer); IR62 (IR thermometer); IRMLX (CWSI Slave station); TCint (RS PRO type T thermocouple); TCext (LI-6400/XT type E thermocouple). The “X” indicates that the measurement was taken with the corresponding instrument/sensor.

Date	Aim	Start	End	Li600	IR62	IRMLX	TCint	TCext
19/07/2022	Mapping	12:12	13:32	X	X	X	-	-
25/07/2022	Mapping	12:27	15:02	X	X	X	-	-
09/08/2022	Mapping	14:30	15:22	X	X	X	-	-
25/08/2022	Calibration	9:37	16:30	X	X	X	X	X
29/08/2022	Calibration	9:32	15:45	X	X	X	X	X

associated with a correspondent value of  $T_{wet}$  and  $T_{dry}$  collected by the CWSI master station, resulting in a CWSI value for every sampled leaf.

### 2.8. Mapping

The measurements collected during the mapping session were associated with the corresponding leaf and position in the vineyard. For every corrected leaf temperature the CWSI value was calculated and plotted in QGIS (Quantum GIS software, QGIS Development Team 2024). Maps of the vineyard for every instrument were created through interpolation using the Inverse Distance Weighting method (IDW) function, available in the QGIS software. The colors of the resulting maps were then divided into intervals to better highlight the distribution of stressed and non-stressed vines.

## 3. RESULTS

### 3.1. Dry and wet reference leaf temperatures

The comparison between the different dry reference temperatures is shown in Fig. 4. The dry reference temperatures chosen for the analysis were the maximum values between the two 3D printed leaves, since the two lines were quite similar, and  $T_{dry}$  should resemble the temperature of a leaf in a non-transpiring state:

$$T_{dry} = \max(T_{CPE}, T_{PA12}) \quad (13)$$

The aluminum disk was discarded because its heat capacity ( $880 \text{ J kg}^{-1} \text{ K}^{-1}$ ) was much lower than the typical heat capacity of a real leaf which usually ranges between  $1287 \text{ J kg}^{-1} \text{ K}^{-1}$  and  $2267 \text{ J kg}^{-1} \text{ K}^{-1}$  (Jayalakashmy and Philip, 2010). Therefore, the heat capacity values of the 3D printed leaves ( $2100 \text{ J kg}^{-1} \text{ K}^{-1}$  for PA12 and  $1300 \text{ J kg}^{-1} \text{ K}^{-1}$  for CPE) were more similar to real leaf values.

The wet bulb temperature of the air was taken as the wet reference temperature ( $T_{wet}$ ) for the calculation of the Crop Water Stress Index. The data collected during the mapping campaign of August 23<sup>rd</sup> are displayed in Fig. 5: the air temperature inside the vineyard resulted to be higher than the air temperature outside the vineyard for all the duration of the campaign and, on the contrary, relative humidity was slightly higher outside the vine rows. The wet bulb temperature of the air, being calculated as a function of these two parameters, was higher inside the vineyard except for the first minutes of the measuring campaign.

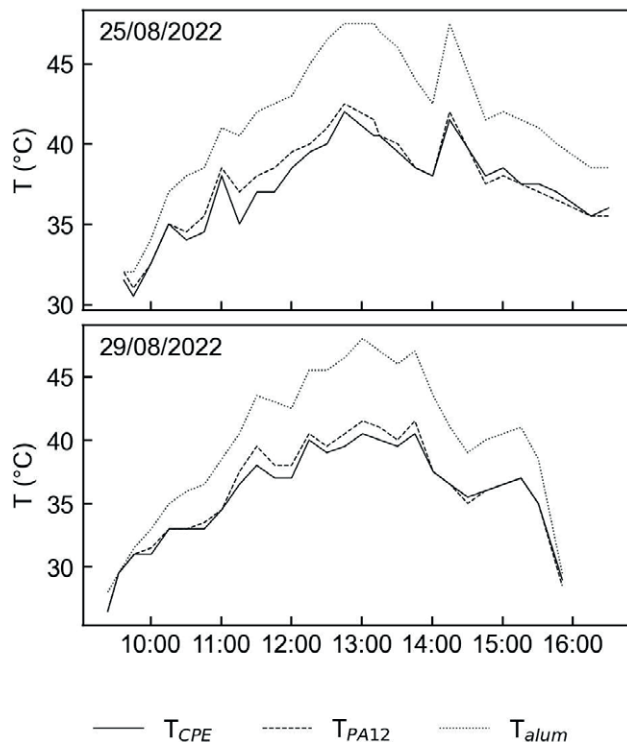


**Figure 4.** Dry reference temperatures measured during the calibration sessions with the CPE 3D printed leaf  $T_{CPE}$ , with the PA12 3D printed leaf ( $T_{PA12}$ ) and with the aluminum oxide disk ( $T_{alum}$ ), are represented respectively by the solid, dashed and dotted line.

### 3.2. Correction of leaf temperatures

Scatter plots of the data collected during the calibration campaigns, comparing temperatures of the different instruments with the internal thermocouple are represented in Fig. 6. The gray line marks the 1:1 reference line and shows how far the measurements were compared to the reference temperature. Basically, all the instruments tended to overestimate leaf temperature especially at the lower values. TCext values almost overlap the 1:1 reference line, therefore showing a very good correspondence with the temperatures measured with the internal thermocouple. Overall, the compared instruments showed quite good slope values, around 0.77 but, in contrast, they presented high intercepts (up to  $11.5 \text{ }^\circ\text{C}$ ). All the relationships were highly significant ( $p < 0.001$ ), with rather high coefficient of determination ( $R^2 > 0.76$ ).

### 3.3. CWSI calculation

Figure 7 displays the CWSI calculated both with measured and corrected temperatures for each day

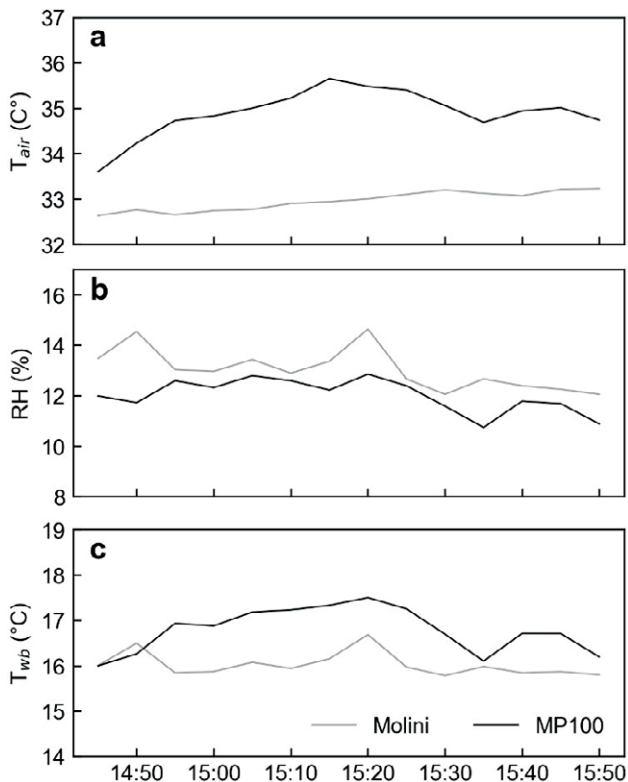


**Figure 5.** Air temperature (a), relative humidity of the air (b) and wet bulb temperature (c), measured with the MP100 thermohygrometer on August 23<sup>rd</sup>. Black line: values measured with the MP100 thermohygrometer; grey line: data recorded by the Molini meteorological station.

of calibration. It is presented as a temporal sequence of CWSI, calculated for the same leaf during the two calibration sessions. On both days all the instruments showed high CWSI values. In some cases, especially during the afternoon, the CWSI values overcame the upper theoretical limit of the index, which is equal to 1. The lowest values of CWSI were recorded on August 25<sup>th</sup> (0.57) and on August 29<sup>th</sup> (0.47). The different temperatures used in the calculation of the CSWI are reported in Fig. 8.

**3.4. Relation between CWSI and stomatal conductance  $g_{sw}$**

The time series of stomatal conductance  $g_{sw}$  and CWSI for the calibration days are reported in Fig. 9. During early morning hours CWSI presented lower values (about 0.6) compared with respect to the central hours of the day, where it varied between 0.8 and 1. The stomatal conductance instead presented higher values around 10:00 ( $g_{sw} = 0.08 \text{ mol m}^{-2} \text{ s}^{-1}$  on August 25<sup>th</sup>,

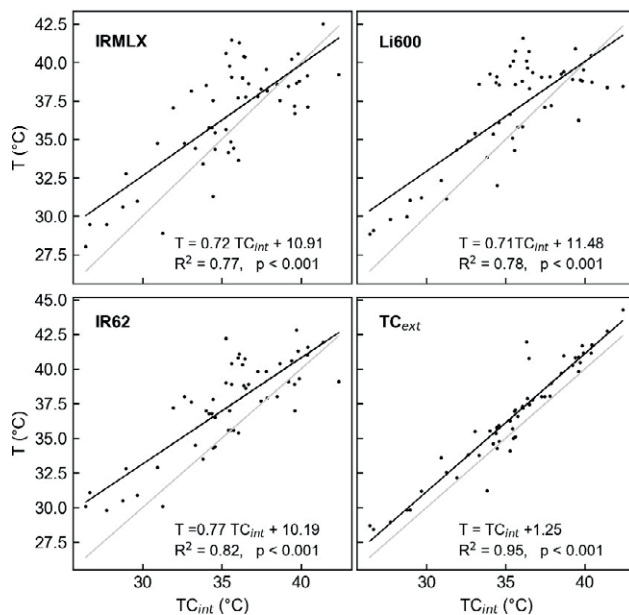


**Figure 6.** Linear regression between the leaf temperatures measured with the internal thermocouple and the other instruments (CWSI Slave station - IRMLX, Licor Porometer-Fluorometer - Li600, Infrared Thermometer - IR62 and thermocouple in contact with the inferior lamina of the leaf - TCext). On the bottom right of every plot are displayed the regression line equation (black line), the coefficient of determination  $R^2$  and the significance  $p$ -value. The gray line is the 1:1 reference line. Each statistic is conducted on a sample of 54 temperature data.

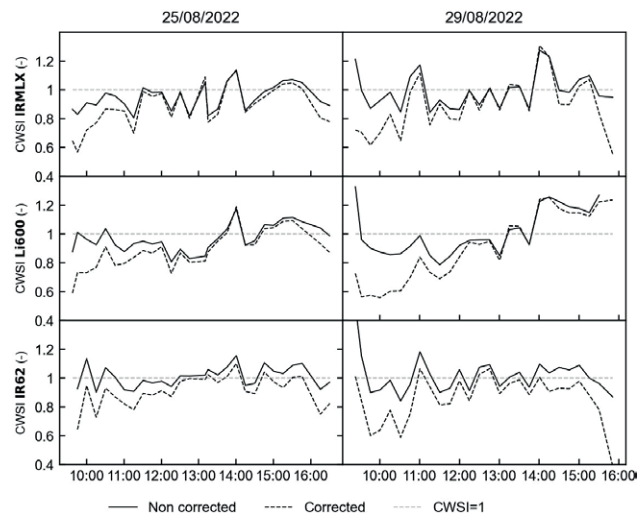


**Figure 7.** CWSIs calculated with the measured temperature (solid line) and with the corrected temperatures (dashed line) of the instruments used in the monitoring sessions for each day of the calibration campaign. The horizontal, dotted line marks the upper theoretical CWSI limit.

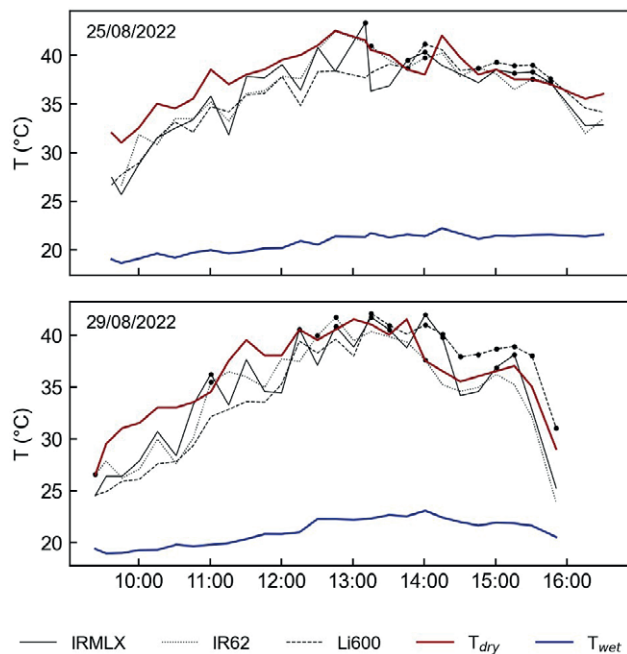


**Figure 8.** Comparison between the two reference baselines  $T_{dry}$  (red) and  $T_{wet}$  (blue) and the leaf temperatures recorded by IRLMX, Li600 and IR62. The dots mark the leaf temperatures higher than  $T_{dry}$ .

and  $g_{sw} = 0.09 \text{ mol m}^{-2} \text{ s}^{-1}$  on August 29<sup>th</sup>) and gradually decreased in the following hours, approaching very low values (almost  $0 \text{ mol m}^{-2} \text{ s}^{-1}$ ).

The relationship between the CWSI and stomatal conductance during the drought period of the summer season came out to be negative (Fig. 10). With CWSI increasing and decreasing  $g_{sw}$ . Every dot in the graph represents the average of CWSI and  $g_{sw}$  of each day of measurement, considering both calibration and mapping sessions. For the mapping sessions the parameters were averaged over the entire vineyard, for the calibration sessions the parameters were averaged over the same leaf and only the data recorded between 12:00 and 15:00 were considered, in order to match the temporal range of the other days.

The stomatal conductance to water vapor also decreased as the summer season progressed, with higher values being recorded in July with respect to the end of August. Consequently, CWSI values appeared to be lower at the beginning of the summer season and then they increased.

### 3.5. QGIS mapping

Interpolation maps were produced for IRLMX and IR62, that were the more accurate instruments in terms of leaf temperature measurement according to the calibration analysis. The maps clearly show the different lev-

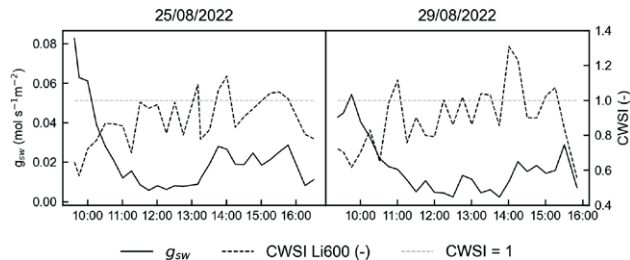


**Figure 9.** Temporal pattern of stomatal conductance  $g_{sw}$  (solid line) and CWSI (dashed line) during the days of calibration. The horizontal dashed line marks the upper theoretical value of CWSI. The values were measured and calculated with the Li600 porometer.

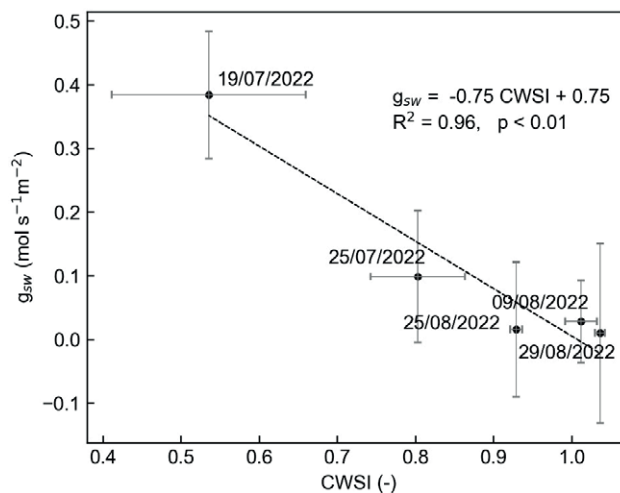


**Figure 10.** Relationship between CWSI (Crop Water Stress Index) and  $g_{sw}$  (stomatal conductance to water vapor) during the summer period of year 2022. Every dot represents an average of both CWSI and  $g_{sw}$  (between 12:00 and 15:00) on a specific day of measurement. Data were fitted with a linear regression line (the regression equation, the coefficient of determination  $R^2$  and significance p-value are reported on the top right of the plot). Bars indicate the error.

els of water stress of the plants in the different areas of the vineyard (Fig. 11). On July 19<sup>th</sup> the values of CWSI remained quite low across the vineyard (Fig. 11 a, b), but the IRLMX map shows how the southern area appears to be slightly more stressed than the northern area (Fig. 11 b); this aspect is not appreciable in the IR62 map (Fig. 11 a). The blue spots (Fig. 11 c, d) represent missing data due probably to a malfunctioning of the instrument. On July 25<sup>th</sup> (Fig. 11 c, d) both maps highlighted two distinct stress areas, with the stress level increasing southward. On the contrary, the northern area of the vineyard appeared to be at a higher stress level on August 9<sup>th</sup>, with high CWSI values almost everywhere (Fig. 11 e, f). The IR62 map (Fig. 11 e) presented higher spatial vari-

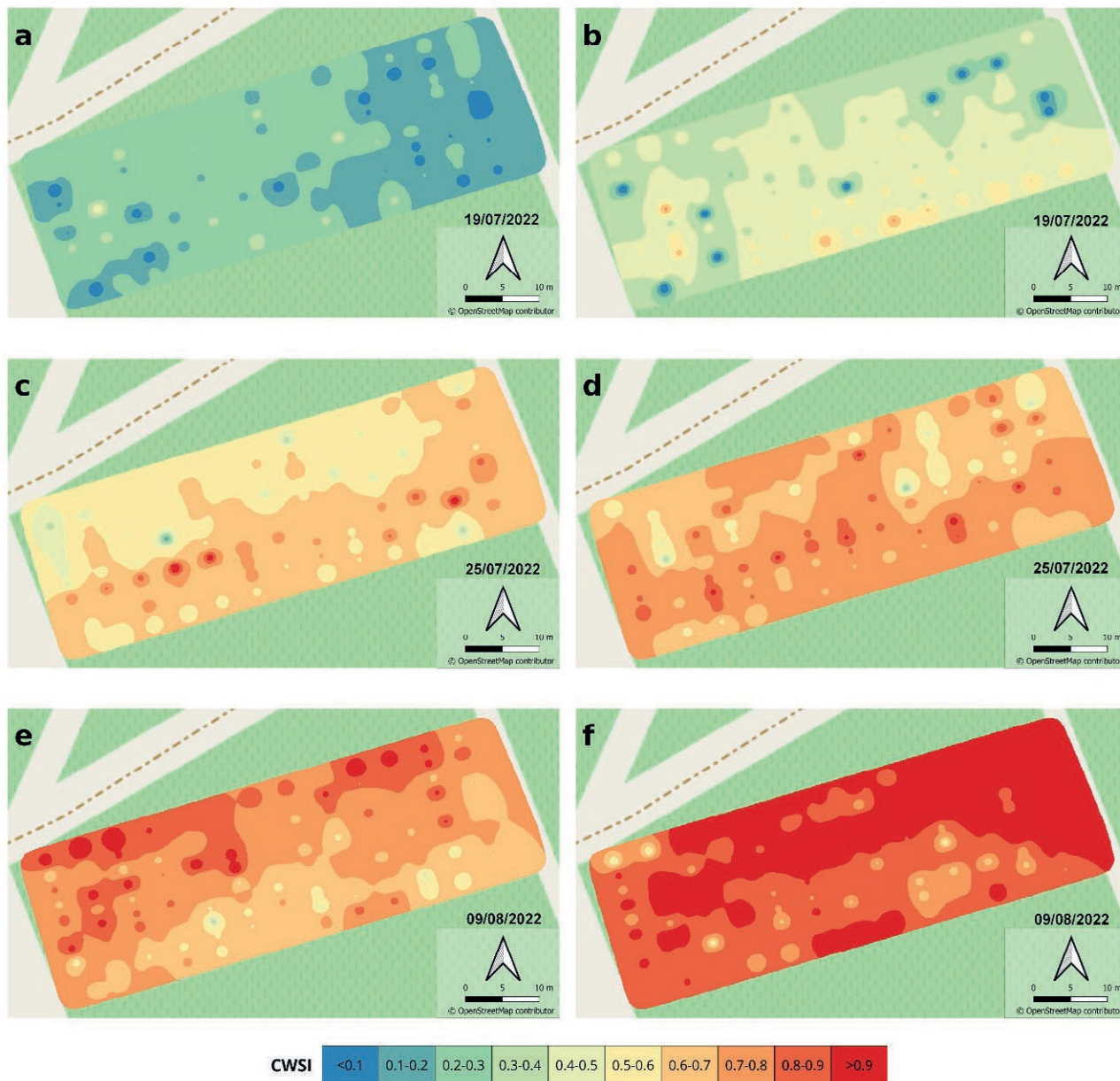


**Figure 11.** Maps of CWSI produced with the data collected during the mapping session of July 19<sup>th</sup>, 2022 (a, b), July 25<sup>th</sup>, 2022 (c, d) and August 9<sup>th</sup>, 2022 (e, f). Every map shows the CWSI calculated with the following instruments: a, c, e: IR62; b, d, f: IRMLX.

ability with respect to the IRMLX one (Fig. 11 f), where the CWSI was at its maximum in most of the vineyard.

#### 4. DISCUSSION

##### 4.1. Leaf temperature correction

The thermocouple inserted in the leaf vein (TCint) was chosen as a reference instrument for the tempera-

ture calibration because in general thermocouples are characterized by good accuracy (0.5 °C) and a short response time given by the low heat capacity of the material (L. Yu et al., 2016). The small size of the thermocouple wire (0.2 mm of diameter) allows an accurate analysis of the small target area of the leaf, also because the sensor does not interfere with the leaf environment.

Furthermore, being in contact with the leaf lamina, it is not influenced by emissivity issues that can instead affect the measurements done with infrared sensors.

Possible sources of error may be due to the absorption of radiation by the thermocouple and to the heat conduction through the wires, but these problems were overcome using low-diameter wires (0.2 mm) and assuring good contact between the wires and the leaf by stripping the insulation off the wires (Tarnopolsky and Seginer, 1999). The instruments compared in this study tended to overestimate the reference leaf temperature, especially at lower temperatures (Fig. 6), whereas there was more scattering towards higher temperatures. As a matter of fact, the three adopted instruments (Li600, IR62, IRMLX) relied on infrared sensors for the detection of object temperatures. Infrared thermometry is usually affected by leaf emission rate and environmental parameters such as dust, carbon dioxide etc. (Yu et al., 2016), or in general by the characteristics of the medium that is present between the measured object and the sensor. Moreover, if the detected temperature is averaged over a large field of view (Halbritter et al., 2020), even less accurate temperature values might be recorded. To minimize this possible source of error, the measurements with IRMLX and IR62 were taken at a distance of about 2-3 cm from the leaf surface.

Another possible reason for the higher temperatures registered by the infrared sensors could be that leaf temperature was measured on the adaxial surface of the leaf, which was directly exposed to the sun. The thermocouple was instead positioned on the abaxial side, which was shaded by the leaf lamina. The difference in radiant energy between the two sides of the leaf could have brought sensible differences in leaf temperature detection (Pallas et al., 1967). The fact that the instrument errors were minimal around solar noon, which is the time of the day when leaf temperatures are generally higher, allowed a better estimation of the water status of the crop. This aspect could be further investigated with measurement of midday leaf water potential using a pressure chamber. This is known to be an effective method to monitor the vine water state but, on the other hand, is an invasive method that relies on appropriate leaf sampling (Deloire et al., 2020). For this reason this kind of analysis was not considered appropriate for this study.

On the other hand, literature suggests that CWSI of a crop should be evaluated between 1 hour and 1:30 hours past solar noon (Idso et al., 1981; Jackson et al., 1981; Bellvert et al., 2014). Infrared thermometers and sensors are widely used nowadays in canopy monitoring (Jackson et al., 1981; Mahan et al., 2010) and are considered one of the most precise and cost-effective leaf temperature measurement methods (Yu et al., 2015; Halbritter et al., 2020). For this reason, they have been considered suitable for the CWSI computation.

#### 4.2. CWSI, dry and wet reference temperatures

The daily trend of CWSI showed low values in the morning, then a gradual increase until 14:00, where it reached the maximum value, followed by a slight decrease in the afternoon (Fig. 10). Irregular peaks were present, probably due to the high variability of the temperature over the leaf surface.

By definition, the index should not be higher than 1, which ideally represents the maximum stressed condition of the plant, but CWSI crossed this upper limit several times in both days and in particular during the afternoon (Fig. 7 and Fig. 8). This issue arises from the empirical determination of the dry reference temperature that should represent the Water-Stressed-Baseline. Indeed, in the calculation of the index (Eq. 7), the result got higher than 1 when the numerator was greater than the denominator, therefore when the actual leaf temperature overcame  $T_{dry}$ . In both days of calibration, after 14:00,  $T_{dry}$  values were lower than the correspondent leaf temperature measured by all the instruments (IR62, IRMLX, Li600) (Fig. 8). This shows that the black 3D printed leaves lost heat faster than the real leaves. So, the dry reference temperature taken as the maximum temperature between the two black 3D-printed leaves was still not the maximum temperature that a leaf can achieve in stress conditions.

The artificial leaves were fixed horizontally, so the orientation could not allow the maximum amount of solar radiation hitting the surface. To improve the estimation of  $T_{dry}$ , a BlackGlobe temperature sensor (Blackglobe-L Campbell Scientific, Logan, UK) could be used; the spherical shape allows the solar beams to hit the surface perpendicularly regardless of the sun elevation, recording higher  $T_{dry}$  values.

Another possible source of uncertainty in the calculation of CWSI could be given by the fact that meteorological parameters measured at the CWSI Master station did not exactly match the meteorological parameters inside the vineyard. As reported in literature (e.g. Peña Quiñones et al., 2020, Matese et al., 2014 and Fig. 5) the air temperature measured inside the canopy can be sensibly higher than the one measured outside. Differences between the inner and outer part of the vineyard are usually present also in relative humidity, that together with air temperature influence the estimation of  $T_{wet}$ . One should expect higher relative humidity values inside the vineyard with respect to the surroundings, given by the transpiration of plants and the evaporation from the soil. However, in this case it was the opposite. RH values were quite low both inside and outside the vineyard, probably due to the hot and sunny meteorological condi-

tions and the fact that plant transpiration was at its minimum around noon.

In order to improve the estimation of the lower baseline temperature, it might be necessary to set the CWSI master station inside the vineyard, in order to increase the accuracy in the measurement of the microclimate of the vineyard canopy. For this study the CWSI master station was installed outside the vineyard in order not to interfere with the regular maintenance activities of the crop that have to be carried out by means of tractors and heavy machines. It was installed as close as possible to the vines, to give the most reliable picture of the microclimate in the proximity of the vineyard.

#### 4.3. Relation between CWSI and stomatal conductance $g_{sw}$

The plot in Fig. 9, showing CWSI against  $g_{sw}$ , is directly comparable with the graph taken by Karaka et al. (2018), displaying seasonal averaged CWSI and  $g_{sw}$  values for soybean cultivars. Both fitting linear regression lines present negative slope (equal to  $-0.66$  for Karaka et al. (2018) and equal to  $-0.75$  for this analysis) and a positive intercept (of  $0.75$  and  $0.65$  for the study of Karaka et al. (2018) and this study respectively).

Stomatal conductance decreased with the progression of the growing season. In July  $g_{sw}$  measured  $0.38 \text{ mol H}_2\text{O m}^{-2} \text{ s}^{-1}$  and at the end of August it approached stomatal inactivity with  $0.009 \text{ mol H}_2\text{O m}^{-2} \text{ s}^{-1}$ . Similarly, Karaka et al., (2018) observed higher values of soybean  $g_{sw}$  at the beginning of the summer season (around  $0.8 \text{ mol H}_2\text{O m}^{-2} \text{ s}^{-1}$ ), and a gradual decline in July and August (reaching values close to  $0.3 \text{ mol H}_2\text{O m}^{-2} \text{ s}^{-1}$ ). This can be also a consequence of the hot and dry climate of their experimental site, that records lower values of precipitation and higher air temperatures during the growing season with respect to the San Michele all’Adige in the same period. At the study site the average precipitation of the growing season is equal to  $540 \pm 151 \text{ mm}$  and the mean air temperature is  $18.7 \pm 6.3 \text{ }^\circ\text{C}$  (data were collected from the meteorological station of Fondazione E. Mach located in S. Michele all’Adige, in the time period going from April to October in the years between 1983 and 2013), whereas at the Turkish experimental site precipitation it is only  $137 \text{ mm}$  and air temperatures set on an average of  $24.5 \text{ }^\circ\text{C}$  (calculated in the time period between 1954 and 2013 (Karaka et al., 2018)). Also Ru et al. (2020) highlighted the increasing trend of CWSI for grapevine through the growing season, that went from  $0.4$  to  $0.8$  for crops cultivated with a deficit irrigation approach. The discrepancies between the correlations could be due to the comparison between different cultivars, and the influence of external factors

such as air temperature (mean air temperature during the growing season was equal to  $21.5 \text{ }^\circ\text{C}$ ), net radiation, wind speed and vapor pressure deficit of the air. Despite these correspondences in the literature, the seasonal pattern of CWSI could be studied more consistently with a higher number of measurement sessions distributed over a longer period of time during the water stressed periods of the growing season.

#### 4.4. QGIS maps

In all the survey days the site of measurement presented spatial variability in terms of CWSI (Fig. 11). The difference in magnitude between the IR62 maps and the IRMLX maps was a common pattern observed in all the field sessions, with the IRMLX maps showing higher values of CWSI in all the mapping campaigns. All the maps in general agreed in the spatial distribution of water stress in the field.

On July 19<sup>th</sup> the IR62 recorded a low, almost uniform stress state, with  $\text{CWSI} < 0.5$ . The IRMLX map shows a slightly higher stress status on the southern side of the vineyard. The low stress state of the field was probably due to the fact that the site was under irrigation on that day and this is reflected by the high values of stomatal conductance with an average value equal to  $0.4 \text{ mol H}_2\text{O m}^{-2} \text{ s}^{-1}$ , that corresponds to the mean value of non-stressed grapevine in that area (Faralli M., personal communication). The appreciable difference in spatial distribution of the maps on July 25<sup>th</sup> is probably due to the different time at which the two areas were sampled: the first 6 rows were mapped between 12:00 and 13:00 and the others were mapped starting from 14:00. As pointed out in the result section, CWSI usually reached its maximum around 14:00, so the values measured in the second part of the day could have been affected by the increase in air temperature and net radiation. The maps of August 9<sup>th</sup> presented the opposite spatial trend compared to the other days, with the northern area of the vineyard more stressed than the southern part. In this day values of CWSI were high everywhere, and this is confirmed by both maps.

To sum up, the spatial differences between the northern and southern area of the vineyard were highlighted by both the instruments for all the monitoring days. This could be a result of the length of the campaign: in fact, during a 1 hour-long campaign, a consistent variation of leaf temperature, air temperature and air relative humidity (and as a consequence of CWSI) can not be totally excluded.

The temporal variability of meteorological variables could be reduced with a faster data collection by

means of Unmanned Aerial Vehicles (UAV), that can be equipped with thermal sensors to obtain the temperature of the target object and are therefore a viable tool to monitor large field areas in a short amount of time. They have the potential to be part of an IoT network, and can give a significant contribution for the development of solutions for irrigation management (Ahansal et al., 2022). Moreover in the guyot pruning system, shoots grow mainly in the vertical direction, having only a small fraction of canopy visible from above. For this reason, the use of UAV could be more suitable for training systems with a canopy more developed in the horizontal plane (i.e. "Pergola" training system), being more easily scanned from above.

Agricultural vehicles, if equipped with thermal cameras or an array of infrared temperature sensors, can be another alternative to ground surveys, that can be time consuming especially for large vineyards (Meron et al., 2010; Zhou et al., 2022). Another viable and non-invasive alternative could be the use of remote sensing technology, which is rapidly increasing nowadays and it is often used in precision agriculture applications. The remote sensing method has the advantage of detecting the spatial variability of the vineyard water status without the need to install an elevated number of on-site sensors in the field. Furthermore, it is applicable at larger scale, and can be implemented both in mountain areas and extensively cultivated plains (Matese et al., 2018). A comparison between CWSI and soil maps could lead to more useful results in terms of irrigation needs. Different stress level areas could also reflect different soil characteristics. The soils ability to retain water is strongly related to soil particle size: sandy soils, with coarser particles, present low water retention capacity whereas deep soils of fine texture can retain higher amounts of water that can be available for plant root uptake (Saxton and Rawls, 2006). However soil maps are not always available and soil monitoring is expensive and time consuming both in terms of physicochemical characteristics and water content.

Maps provide valuable visual information about the state of the vineyard and can be of great help for farmers in the assessment of the crop water status and management of the water resource. The spatial interpolation allows to identify areas with different water stress characteristics, that could then be handled in different ways in terms of irrigation management, applying different amounts of water (Meron et al., 2010). Following the approach proposed in this study, CWSI maps could be obtained to give practical support for irrigation management, therefore saving water and increasing water use efficiency.

## 5. CONCLUSIONS

In a period of climate change, characterized by extreme events, prolonged drought periods are posing serious problems to the management of crops. Therefore, precision agriculture can provide the tools to optimize the use of water with the aim to increase water use efficiency. In this study, a new approach for the calculation of the Crop Water Stress Index was tested, based on the empirical formulation of the index proposed by Idso et al. (1981) and Jackson et al. (1981). Overall, the applied approach gave quite good results allowing the creation of maps by which it was possible to differentiate among areas within the vineyard presenting different levels of stress and therefore being of great help in the management of irrigation. Some technical aspects need to be improved in order to increase the accuracy in the calculation of the index: the maximum leaf temperature resulted to be slightly underestimated. Therefore, the use of a BlackGlobe sensor mimicking a non-transpiring leaf could help in the correct quantification of the radiation absorbed by a leaf at changing solar zenith angles. The IR sensors used in the measurement of the leaf temperature tended to overestimate its value: a contact thermocouple integrated into the CWSI slave station could give more reliable results. Finally, the master station should be positioned inside the vineyard in order to better represent the canopy microclimate which can be slightly different from the outside. IoT connectivity played a primary role in the present work: thanks to it, every leaf measurement performed with the IRMLX could be associated with the corresponding values of  $T_{dry}$  and  $T_{wet}$ , and the CWSI was automatically calculated. In conclusion, the present study confirmed the validity of the approach, and highlighted some weaknesses that can be solved in order to improve the estimation of the CWSI.

## REFERENCES

- Adams R., Hurd B., Lenhart S., Leary N., 1998. Effects of global climate change on world agriculture: an interpretive review. *Climate Research* 11: 19–30.
- Ahansal Y., Bouziani M., Yaagoubi R., Sebari I., Sebari K., Kenny L., 2022. Towards Smart Irrigation: A Literature Review on the Use of Geospatial Technologies and Machine Learning in the Management of Water Resources in Arboriculture. *Agronomy* 12 (2): 297.
- Apolo-Apolo O., Martínez-Guanter J., Pérez-Ruiz M., Egea G., 2020. Design and assessment of new artificial reference surfaces for real time monitoring of

- crop water stress index in maize. *Agricultural Water Management* 240: 106304.
- Bellvert J., Zarco-Tejada P.J., Girona J., Fereres E., 2014. Mapping crop water stress index in a ‘Pinot-noir’ vineyard: comparing ground measurements with thermal remote sensing imagery from an unmanned aerial vehicle. *Precision Agriculture* 15 (4): 361–376.
- Buckley T.N., 2019. How do stomata respond to water status? *New Phytologist* 224 (1): 21–36.
- Bwambale E., Abagale F.K., Anornu G.K., 2022. Smart irrigation monitoring and control strategies for improving water use efficiency in precision agriculture: A review. *Agricultural Water Management* 260: 107324.
- Caffarra A. and Eccel E., 2011. Projecting the impacts of climate change on the phenology of grapevine in a mountain area: Effects of climate change on grape phenology. *Australian Journal of Grape and Wine Research* 17 (1): 52–61.
- Change C.C. and Services A.M., 2024. *Global Climate Highlights Report 2023*. English.
- Chaves M., Costa J., Zarrouk O., Pinheiro C., Lopes C., Pereira J., 2016. Controlling stomatal aperture in semi-arid regions—The dilemma of saving water or being cool? *Plant Science* 251: 54–64.
- Deloire A., Pellegrino A., Rogiers S., 2020. A few words on grapevine leaf water potential. *IVES Technical Reviews, vine and wine*.
- Esposito M., Palma L., Belli A., Sabbatini L., Pierleoni P., 2022. Recent Advances in Internet of Things Solutions for Early Warning Systems: A Review. *Sensors* 22 (6): 2124.
- Fuentes-Peñailillo F., Ortega-Farías S., Acevedo-Opazo C., Rivera M., Araya-Alman M., 2024. A Smart Crop Water Stress Index-Based IoT Solution for Precision Irrigation of Wine Grape. *Sensors* 24 (1).
- Halbritter A.H., De Boeck H.J., Eycott A.E., Reinsch S., Robinson D.A., Vicca S., Berauer B., Christiansen C.T., Estiarte M., Grünzweig J.M., Gya R., Hansen K., Jentsch A., Lee H., Linder S., Marshall J., Pen˜ uelas J., Kappel Schmidt I., Stuart-Haeˆntjens E., Wilfahrt P., the ClimMani Working Group, Vandvik V., 2020. The handbook for standardized field and laboratory measurements in terrestrial climate change experiments and observational studies (ClimEx). *Methods in Ecology and Evolution* 11 (1). Ed. by Freckleton R.: 22–37.
- Idso, 1982. Non-water-stressed baselines: A key to measuring and interpreting plant water stress. *Agricultural Meteorology* 27 (1-2): 59–70.
- Idso, Jackson R., Pinter P., Reginato R., Hatfield J., 1981. Normalizing the stress-degree-day parameter for environmental variability. *Agricultural Meteorology* 24: 45–55.
- Intergovernmental Panel On Climate Change (IPCC), 2023. *Climate Change 2022 – Impacts, Adaptation and Vulnerability: Working Group II Contribution to the Sixth Assessment Report of the Intergovernmental Panel on Climate Change*. 1st ed. Cambridge University Press.
- Jackson R.D., Idso, Reginato R.J., Pinter P.J., 1981. Canopy temperature as a crop water stress indicator. *Water Resources Research* 17 (4): 1133–1138.
- Jayalakshmy M.S. and Philip J., 2010. Thermophysical Properties of Plant Leaves and Their Influence on the Environment Temperature. *International Journal of Thermophysics* 31 (11-12): 2295–2304.
- Jones H.G., 1999. Use of infrared thermometry for estimation of stomatal conductance as a possible aid to irrigation scheduling. *Agricultural and Forest Meteorology* 95 (3): 139–149.
- Jones H.G., Hutchinson P.A., May T., Jamali H., Deery D.M., 2018. A practical method using a network of fixed infrared sensors for estimating crop canopy conductance and evaporation rate. *Biosystems Engineering* 165: 59–69.
- Karaka C., Tekelioglu B., Buyuktas D., Bastug R., 2018. Relations between Crop Water Stress Index and stomatal conductance of soybean depending on cultivars. *Fresenius Environmental Bulletin* 27. Edition: 27 Section: 6: 4212–4219.
- Katimbo A., Rudnick D.R., DeJonge K.C., Lo T.H., Qiao X., Franz T.E., Nakabuye H.N., Duan J., 2022. Crop water stress index computation approaches and their sensitivity to soil water dynamics. *Agricultural Water Management* 266: 107575.
- Kim Y., Still C.J., Roberts D.A., Goulden M.L., 2018. Thermal infrared imaging of conifer leaf temperatures: Comparison to thermocouple measurements and assessment of environmental influences. *Agricultural and Forest Meteorology* 248: 361–371.
- King B.A., Shellie K.C., 2023. A crop water stress index based internet of things decision support system for precision irrigation of wine grape. *Smart Agricultural Technology* 4: 100202.
- Lawrence M.G., 2005. The Relationship between Relative Humidity and the Dewpoint Temperature in Moist Air: A Simple Conversion and Applications. *Bulletin of the American Meteorological Society* 86 (2): 225–234.
- Leinonen I., Jones H.G., 2004. Combining thermal and visible imagery for estimating canopy temperature and identifying plant stress. *Journal of Experimental Botany* 55 (401): 1423–1431.
- Maes W.H., Baert A., Huete A.R., Minchin P.E., Snelgar W.P., Steppe K., 2016. A new wet reference target method for continuous infrared thermography

- of vegetations. *Agricultural and Forest Meteorology* 226-227: 119–131.
- Mahan J.R., Conaty W., Neilsen J., Payton P., Cox S.B., 2010. Field performance in agricultural settings of a wireless temperature monitoring system based on a low-cost infrared sensor. *Computers and Electronics in Agriculture* 71 (2): 176–181.
- Martínez J., Egea G., Agüera J., Pérez-Ruiz M., 2017. A cost-effective canopy temperature measurement system for precision agriculture: a case study on sugar beet. *Precision Agriculture* 18 (1): 95–110.
- Matese A., Baraldi R., Berton A., Cesaraccio C., Di Gennaro S.F., Duce P., Facini O., Mameli M.G., Piga A., Zaldei A., 2018. Estimation of Water Stress in Grapevines Using Proximal and Remote Sensing Methods. *Remote Sensing* 10 (1): 159–167.
- Matese A., Crisci A., Di Gennaro S.F., Primicerio J., Tomasi D., Marcuzzo P., Guidoni S., 2014. Spatial variability of meteorological conditions at different scales in viticulture. *Agricultural and Forest Meteorology* 189-190: 159–167.
- Mathur S., Agrawal D., Jajoo A., 2014. Photosynthesis: Response to high temperature stress. *Journal of Photochemistry and Photobiology B: Biology* 137: 116–126.
- Meron M., Tsipris J., Orlov V., Alchanatis V., Cohen Y., 2010. Crop water stress mapping for site-specific irrigation by thermal imagery and artificial reference surfaces. *Precision Agriculture* 11 (2): 148–162.
- Nair S., Johnson J., Wang C., 2013. Efficiency of Irrigation Water Use: A Review from the Perspectives of Multiple Disciplines. *Agronomy Journal* 105 (2): 351–363.
- Nanda M.K., Giri U., Bera N., 2018. Canopy Temperature-Based Water Stress Indices: Potential and Limitations. In: *Advances in Crop Environment Interaction*. Ed. by Bal S.K., Mukherjee J., Choudhury B.U., Dhanwan A.K. Singapore: Springer Singapore, 365–385.
- Ouerghi F., Ben-Hammouda M., Teixeira Da Silva J., Albouchi A., Bouzaïen G., Aloui S., Cheikh-M'Hamed H., Nasraoui B., 2014. The effects of vapor guard on some physiological traits of durum wheat and barley leaves under water stress. *Agriculturae Conspectus Scientificus* 79 (4): 261–267.
- Pallas J.E., Michel B.E., Harris D.G., 1967. Photosynthesis, Transpiration, Leaf Temperature, and Stomatal Activity of Cotton Plants under Varying Water Potentials. *Plant Physiology* 42 (1): 76–88.
- Peña Quiñones A.J., Hoogenboom G., Salazar Gutiérrez M.R., Stöckle C., Keller M., 2020. Comparison of air temperature measured in a vineyard canopy and at a standard weather station. *PLOS ONE* 15 (6). Ed. by Huang M.: e0234436.
- Poblete-Echeverría C., Espinace D., Sepúlveda-Reyes D., Zúñiga M., Sanchez M., 2017. Analysis of crop water stress index (CWSI) for estimating stem water potential in grapevines: comparison between natural reference and baseline approaches. *Acta Horticulturae* (1150): 189–194.
- Poirier-Pocovi M., Bailey B.N., 2020. Sensitivity analysis of four crop water stress indices to ambient environmental conditions and stomatal conductance. *Scientia Horticulturae* 259: 108825.
- Ru C., Hu X., Wang W., Ran H., Song T., Guo Y., 2020. Evaluation of the Crop Water Stress Index as an Indicator for the Diagnosis of Grapevine Water Deficiency in Greenhouses. *Horticulturae* 6 (4): 86.
- Saxton K.E., Rawls W.J., 2006. Soil Water Characteristic Estimates by Texture and Organic Matter for Hydrologic Solutions. *Soil Science Society of America Journal* 70 (5): 1569–1578.
- Stull R., 2011. Wet-Bulb Temperature from Relative Humidity and Air Temperature. *Journal of Applied Meteorology and Climatology* 50 (11): 2267–2269.
- Tarnopolsky M., Seginer I., 1999. Leaf temperature error from heat conduction along thermo-couple wires. *Agricultural and Forest Meteorology* 93 (3): 185–194.
- Venios X., Korkas E., Nisiotou A., Banilas G., 2020. Grapevine Responses to Heat Stress and Global Warming. *Plants* 9 (12): 1754.
- Wu J., Wang J., Hui W., Zhao F., Wang P., Su C., Gong W., 2022. Physiology of Plant Responses to Water Stress and Related Genes: A Review. *Forests* 13 (2): 324.
- Yu, Ding G.-D., Gao G.-L., Zhao Y.-Y., Yan L., Sai K., 2015. Using Plant Temperature to Evaluate the Response of Stomatal Conductance to Soil Moisture Deficit. *Forests* 6 (12): 3748–3762.
- Yu L., Wang W., Xin Z., Zheng W., 2016. A Review on Leaf Temperature Sensor: Measurement Methods and Application. In: vol. 478.
- Zhao W., Liu L., Shen Q., Yang J., Han X., Tian F., Wu J., 2020. Effects of Water Stress on Photosynthesis, Yield, and Water Use Efficiency in Winter Wheat. *Water* 12 (8): 2127.
- Zhou Z., Diverres G., Kang C., Thapa S., Karkee M., Zhang Q., Keller M., 2022. Ground-Based Thermal Imaging for Assessing Crop Water Status in Grapevines over a Growing Season. *Agronomy* 12 (2): 322.